nature communications

Article

https://doi.org/10.1038/s41467-025-55844-8

The assembly factor Reh1 is released from the ribosome during its initial round of translation

Received: 27 November 2023

Accepted: 23 December 2024

Published online: 03 February 2025

Check for updates

Sharmishtha Musalgaonkar[1,5,8], James N. Yelland[2,6,8], Ruta Chitale[2], Shilpa Rao[1], Hakan Ozadam[1,7], David W. Taylor[1,2,3,4], Can Cenik[1] & Arlen W. Johnson[1,2]

Assembly of functional ribosomal subunits and successfully delivering them to the translating pool is a prerequisite for protein synthesis and cell growth. In *S. cerevisiae*, the ribosome assembly factor Reh1 binds to pre-60S subunits at a late stage during their cytoplasmic maturation. Previous work shows that the C-terminus of Reh1 inserts into the polypeptide exit tunnel of the pre-60S subunit. Here, we show that Reh1-bound nascent 60S subunits associate with 40S subunits to form actively translating ribosomes. Using selective ribosome profiling, we found that Reh1-bound ribosomes populate open reading frames near start codons. Reh1-bound ribosomes are also strongly enriched for initiator tRNA, indicating they are associated with early elongation. Using cryo-electron microscopy to image Reh1-bound 80S ribosomes, we found they contain A site peptidyl tRNA, P site tRNA and eIF5A, indicating that Reh1 does not dissociate from 60S until translation elongation. We propose that Reh1 is displaced by the elongating peptide chain, making it the last assembly factor released from the nascent 60S subunit during its initial round of translation.

In eukaryotic cells, ribosome synthesis begins co-transcriptionally in the nucleolus. Early events of rRNA processing and RNA folding in the nucleolus culminate in the release of pre-40S and pre-60S subunits into the nucleoplasm, where they are then independently exported to the cytoplasm (see[1–4] for recent reviews). Although the nascent subunits are largely assembled prior to nuclear export, they must undergo key cytoplasmic assembly events to become functional ribosomal subunits[5,6]. These cytoplasmic assembly events include completion of the peptidyl transfer center. In addition to final assembly events, an entourage of assembly factors that block critical ligand binding sites on the ribosomal subunits must be removed to allow the ribosome to function in translation[7]. Notably, the nuclear export adapter Nmd3 occupies the P and E sites, Tif6 binds to the joining face, thereby preventing association with a small subunit, and the GTPase Nog1, which occupies the A site, also extends around the subunit and inserts into the polypeptide exit tunnel (PET)[8].

In the cytoplasm, maturation of the pre-60S complex follows distinct hierarchical pathways[9], which converge on a pre-60S intermediate bound by the ribosome assembly factors Nmd3, Tif6 and Reh1 (Fig. 1a)[10]. One branch of this pathway involves protein exchanges at the PET. Because the C-terminus of Nog1 is intertwined with Rlp24, the release of Rlp24 is thought to simultaneously extract Nog1 from the PET[11]. Subsequently, Rei1 binds to the subunit and like Nog1, the C-terminus of Rei1 inserts into the exit tunnel[12]. The mechanism by which Rei1 is removed is not clearly understood, although it may be released in conjunction with Arx1 by the Hsp70 Ssa1/2[12–14]. In yeast, Rei1

[1]Department of Molecular Biosciences, The University of Texas at Austin, Austin, USA. [2]Interdisciplinary Life Sciences Graduate Program, The University of Texas at Austin, Austin, USA. [3]Center for Systems and Synthetic Biology, The University of Texas at Austin, Austin, USA. [4]Livestrong Cancer Institutes, Dell Medical School, Austin, USA. [5]Present address: SalioGen Therapeutics, Lexington, USA. [6]Present address: Basic Sciences Division and Computational Biology Section of the Public Health Sciences Division, Fred Hutchinson Cancer Center, Seattle, USA. [7]Present address: Senda Biosciences, Cambridge, USA. [8]These authors contributed equally: Sharmishtha Musalgaonkar, James N. Yelland. e-mail: ccenik@austin.utexas.edu; arlen@utexas.edu

https://doi.org/10.1038/s41467-025-55844-8

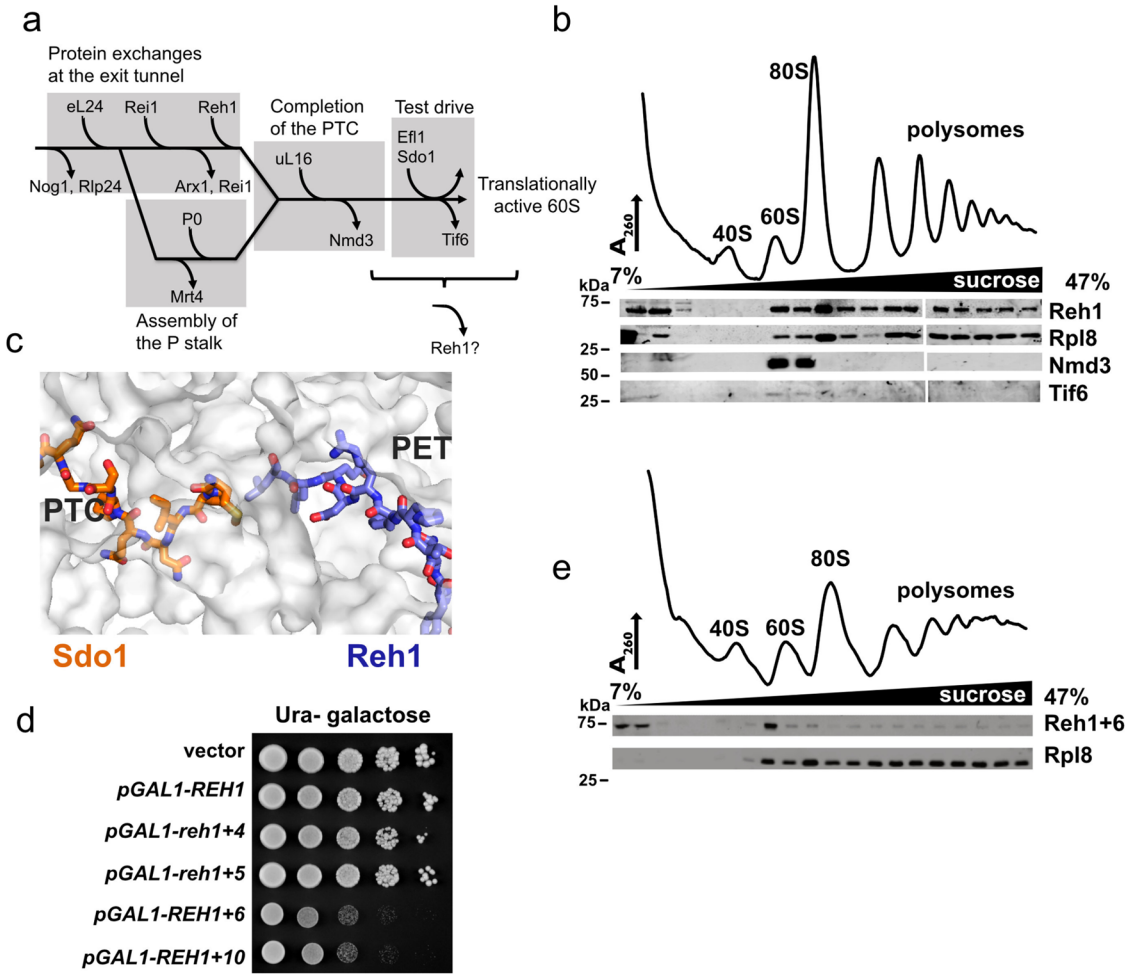

Fig. 1 | Reh1 remains associated with 60S during the transition from biogenesis to translation. a Simplified pathway of cytoplasmic 60S maturation. The major events at the exit tunnel, assembly of the P-stalk, completion of the peptidyl transferase center (PTC) and the test drive to license the subunit are shown. **b** Reh1 sediments into polysomes. Extract of WT cells (AJY4408) expressing 3xmyc-tagged Reh1 (pAJ4763) was separated by sucrose density gradient sedimentation. UV trace monitoring A_{260} is shown. Fractions were analyzed by western blotting for the presence of Reh1, Rpl8 and Nmd3. **c** Cartoon depicting the expected relationship of the N-terminus of Sdo1[60] and the C-terminus of yeast Reh1 in the PET of the 60S subunit. The N-terminus of yeast Sdo1 was modeled on human SBDS (PDB 6qkl)[60] and aligned to yeast pre-60S containing Reh1 (6qt0)[5]. **d** *REH1 + 6* is dominant negative. Ten-fold serial dilutions of wild-type yeast (BY4741) containing vector (pRS416), or galactose-inducible WT *REH1* (pAJ4763) or *REH1* with the indicated number of amino acids from the N-terminus of Sdo1 fused to the C-terminus of Reh1, plated on galactose-containing media. **e** Reh1 + 6 does not enter polysomes. Extract of cells expressing *REH1 + 6* (pAJ4764) was separated by sucrose density gradient sedimentation. UV trace and the sedimentation of Reh1 + 6 and Rpl8 are shown. Experiments shown in panels b and d are representative of at least three independent experiments with similar results. The experiment shown in panel e is representative of two independent experiments with similar results. Source data are provided as a Source Data file.

has a paralog, Reh1, which replaces Rei1 at the time of Arx1 release[5]. Reh1 and Rei1 are functionally redundant[15] and, as with Rei1, the C-terminus of Reh1 inserts into the exit tunnel[5,10]. In parallel with events at the exit tunnel, the peptidyl transferase center is completed by the insertion of uL16 (Rpl10)[5,6]. Accommodation of uL16 triggers the release of Nmd3 from the P and E sites, allowing the P site ligand Sdo1 to bind. Sdo1 activates the GTPase Efl1 to release Tif6 from the nascent subunit[16], thereby licensing the subunit for translation. We previously showed that Efl1 is sensitive to perturbations in the P site[17], and proposed that the Efl1-dependent release of Tif6 represents a "test drive" of the subunit. This process simultaneously assesses the assembly of the P stalk and the integrity of the P site.

The release of Tif6 is currently thought to be the last step of 60S maturation, releasing a fully mature ribosome, free of assembly factors, into the translating pool. However, the timing and mechanism of release of Reh1 have not been examined. While the C-terminus of Reh1 occupies the exit tunnel, the N-terminus of Reh1 is thought to interact directly with Tif6[5], leading to the notion that Reh1 is released in conjunction with Tif6. This idea is supported by structural analysis, which identified a late maturation intermediate containing Tif6 and Reh1, but lacking Nmd3 and Lsg1[5]. Here, we show that Reh1 is released not only after Tif6, but after translation initiation. In particular, our results suggest that Reh1 is released at an early stage of translation elongation, possibly triggered by the nascent polypeptide. Our findings identify Reh1 as a non-canonical ribosome assembly factor that remains associated with the nascent subunit through translation initiation and uniquely marks the initial round of translation for the newly made 60S subunit.

Results

Reh1 sediments with free 60S subunits and polysomes

Mass spectrometric and cryo-EM analyzes have identified Reh1 as a late 60S assembly factor that joins the pre-60S after the release of its paralog, Rei1, in the cytoplasm[5,10,18]. As the release of Tif6 licenses pre-60S for translation by relieving the block in joining to 40S, the release of Tif6 has been assumed to be the last step of 60S maturation (Fig. 1a).

However, the timing of Reh1 release relative to Tif6 release remains unknown. We monitored the sedimentation of Reh1 in sucrose density gradients to determine if it behaved as other canonical pre-60S factors which sediment exclusively with pre-60S. In contrast to Nmd3 and Tif6, which co-sedimented only with free 60S subunits, transiently expressed FLAG-tagged Reh1 was present in polysome-containing fractions in addition to the free 60S fraction (Fig. 1b). A similar sedimentation pattern has been reported for REIL1, the presumed *A. thaliana* homolog of Reh1[19]. Reh1 expressed from its endogenous locus also sedimented into polysomes (Supplementary Fig. 1A) but shifted to free 60S upon inhibition of translation initiation by glucose depletion (Supplementary Fig. 1b). These results reveal that Reh1 persists on 60S subunits after subunit joining, suggesting that it is released after Tif6.

Reh1 progresses from pre-60S into polysomes

The association of Reh1 with 60S subunits as they enter the translation cycle could alternatively be explained by Reh1 entering polysomes by binding to recycling mature subunits. To ask if Reh1 enters polysomes exclusively through the biogenesis pathway, we generated an Reh1 mutant that would block the progression of nascent 60S into the pool of actively translating ribosomes. We reasoned that extending the C-terminus of Reh1, which inserts into the polypeptide exit tunnel, would block Sdo1 binding and arrest 60S maturation at the point of Tif6 release. To this end, we extended the C-terminus of Reh1 with four, five, six or ten residues from the N-terminus of Sdo1, which inserts into the exit tunnel from the joining face (Fig. 1c). Overexpression of variants with four or five residue extensions had no adverse effect on cell growth, but variants extended by six (*REH1 + 6*) or ten (*REH1 + 10*) residues had a potent dominant negative effect when overexpressed (Fig. 1d). As predicted, the sedimentation of Reh1 + 6 was heavily enriched in pre-60S (Fig. 1e). The absence of Reh1 + 6 from 80S and polysome fractions strongly suggests that this protein does not bind to recycling 60S, supporting our conclusion that WT Reh1 enters polysomes through the biogenesis pathway.

A dominant mutant of Reh1 blocks the release of Nmd3 and Tif6

We expected Reh1 + 6 to block Sdo1 binding, thereby inhibiting the release of Tif6 by the GTPase Efl1[16]. To directly test if Reh1 + 6 inhibited Efl1 function, we assayed the effect of Reh1 + 6 on the GTPase activity of Efl1 in vitro. As previously reported, Efl1 activity was activated by Sdo1 in the presence of 60S subunits (Fig. 2a)[20]. The addition of wild-type Reh1, at either equimolar or five-fold excess amounts over 60S, did not significantly inhibit Efl1 activity. However, Reh1 + 6 had a dose-dependent inhibitory effect, reducing the GTPase activity of Efl1 more than 50% when Reh1 + 6 was in five-fold excess over 60S subunits (Fig. 2a).

To determine at which step Reh1 + 6 arrested the cytoplasmic maturation pathway in vivo, we examined the cellular localization of assembly factors that shuttle between the nucleus and cytoplasm[9]. Overexpression of the dominant negative *REH1 + 6*, but not WT *REH1*, strongly inhibited nuclear recycling of Tif6 (Fig. 2b). To monitor the recycling of Nmd3, which is cytoplasmic at steady state, we employed the *NMD3-L505A* mutant, which we previously found to have a reduced rate of nuclear export, shifting the steady state distribution of Nmd3 to the nucleus[21]. Overexpression of *REH1 + 6* also strongly inhibited the nuclear recycling of Nmd3-L505A (Fig. 2c). In contrast, overexpression of *REH1 + 6* did not block the recycling of Nog1, Arx1 or Mrt4, which are released from pre-60S in the cytoplasm upstream of the release of Nmd3 and Tif6 (Figs. 1a and 2d)[9]. Thus, Reh1 + 6 specifically blocks a late step in 60S assembly.

Sdo1 and Efl1 are dispensable in the presence of *tif6* mutants that weaken the affinity of Tif6 for pre-60S[20]. We tested if one such mutant, *TIF6-V192F*, could bypass the dominant negative effect of *REH1 + 6*. Indeed, co-expression of *REH1 + 6* with *TIF6-V192F* but not WT *TIF6* largely relieved the dominant negative growth effect of *REH1 + 6* (Fig. 2e). Remarkably, *TIF6-V192F* also allowed Reh1 + 6-containing 60S subunits to enter polysomes (Fig. 2f). These results show that Reh1 + 6 can enter polysomes, but only when the biogenesis arrest is alleviated by mutation of *TIF6*. Taken together, our results indicate that Reh1 is released after Tif6. We conclude that Reh1 is the last biogenesis factor to be released from the 60S subunit, and that its release occurs after subunit joining.

The C-terminus of Reh1 is critical for function and for binding to 60S subunits

Structural studies of pre-60S particles have shown that the extreme C-terminus of Reh1 occupies the PET (Supplementary Fig. 2a), while other regions of Reh1 interact with eL24 and with Tif6 on the joining face[5,10]. Thus, after Tif6 is released, Reh1 may be tethered to the ribosome primarily through the interaction of its C-terminus with the PET and interaction with eL24. To assess the contribution of the C-terminus of Reh1 to ribosome binding, we generated two C-terminal truncations that removed 6 or 43 residues of Reh1, and assayed their sedimentation with ribosomes in sucrose density gradients in vivo. The number of residues deleted was guided by the structure of Reh1 in the PET (Supplementary Fig. 2a). The 6 amino acid deletion removed residues extending to the uL22-uL4 constriction point in the PET, whereas the 43 amino acid deletion removed the entirety of the C-terminus that occupies the exit tunnel. The two truncations differed in their ability to bind to ribosomes: Reh1Δ6 retained ribosome binding, whereas the binding of Reh1Δ43 was significantly impaired (Supplementary Fig. 2b). These results demonstrate that the C-terminal 43 amino acids of Reh1 are important for its association with the ribosome. We also tested the ability of these truncations to complement loss of *REH1*. Because *REH1* is partially redundant with *REI1*[15], we tested complementation in a *reh1Δ rei1Δ* double mutant. However, because Rei1 is needed for the removal of Arx1 from pre-60S[22,23], we also introduced *arx1-S347P*, a mutation which suppresses the growth defect of *rei1Δ* but retains *ARX1* function[9]. We found that deletion of either 6 or 43 amino acids from the C-terminus of Reh1 rendered the protein nonfunctional (Supplementary Fig. 2c). This result was unexpected because deletion of the corresponding regions of Rei1 has little impact on cell growth[24] and suggests that Reh1 function is more dependent on its C-terminus for binding to the pre-60S subunit than is Rei1.

Selective ribosome profiling of Reh1-bound ribosomes

Thus far, our results indicate that Reh1 remains associated with nascent 60S subunits after subunits join during translation initiation. To gain a more complete understanding of when Reh1 is released during the translation cycle, we used selective ribosome profiling to determine where Reh1-containing ribosomes are positioned on mRNAs (Fig. 3a).

The footprints from Reh1-bound ribosomes that mapped to mRNAs displayed a length distribution centered on 28 nt (Fig. 3b), and the vast majority (>97%) originated from coding regions (Fig. 3c). Similar results were obtained with bulk ribosome profiling, (Fig. 3b,c). In addition, ribosome footprint counts per gene had a Spearman correlation of 0.974 and 0.979 between the replicates of selective and conventional ribosome profiling experiments, respectively, illustrating the high quality of these datasets. Both WT Reh1-bound ribosome footprints and footprints from bulk ribosomes displayed clear three nucleotide periodicity (Fig. 3d), indicative of translating ribosomes.

Excitingly, analysis of the Reh1-bound ribosome footprints showed a strong enrichment within the first ~75 nucleotides of open reading frames (ORFs), compared to bulk ribosome footprints, which were uniformly distributed across coding regions (Fig. 3d). We also observed a strong signal for Reh1-bound ribosomes at stop codons (Fig. 3e). This was unexpected and cannot be easily explained by our model that Reh1 engages with ribosomes via the biogenesis pathway,

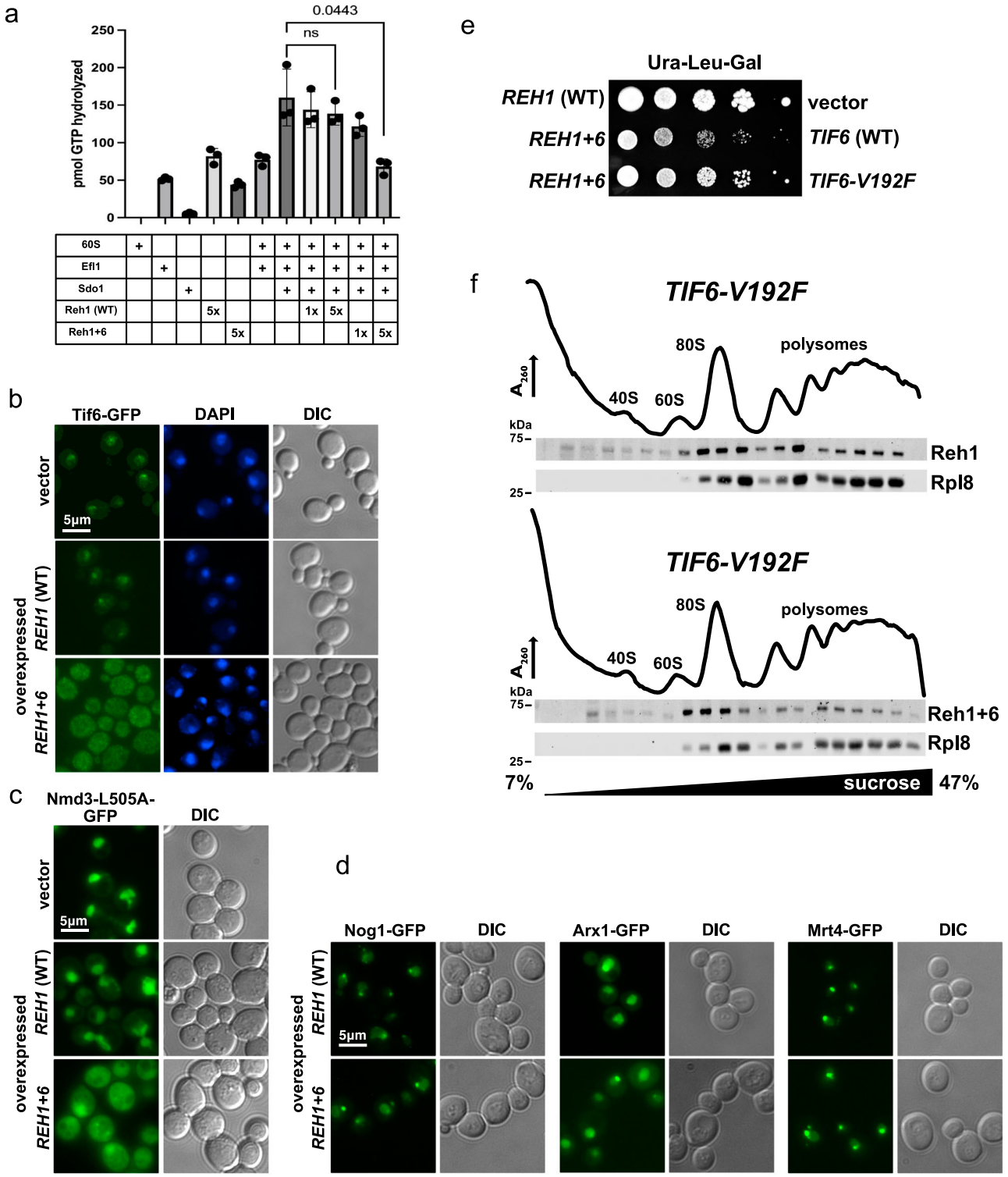

raising the possibility that Reh1 can engage 80S ribosomes post termination. However, we do not see evidence for Reh1 association with terminating ribosomes in our structural work (see below, Cryo-EM structure of the Reh1-80S complex) and it is difficult to conceive of how Reh1 could engage with the exit tunnel on a terminating 80S ribosome.

The strong enrichment of Reh1-bound ribosome footprints at the 5′-end of ORFs is consistent with a model in which Reh1 is released in early rounds of translation as the growing nascent polypeptide encounters the C-terminus of Reh1. Based on the structure of the ribosome, the distance from the PTC to the constriction point in the exit tunnel is about 30 Å which can accommodate a polypeptide of 10–20 residues[25,26]. As it is likely that the growing nascent polypeptide would be incompatible with the C-terminus of Reh1 at the constriction point in the PET, Reh1 would have to be released for the nascent peptide to extend beyond the constriction point. The ability to accommodate 10-20 residues of nascent chain before Reh1 eviction correlates well with our Reh1 footprinting results which show enrichment in the first 25 codons (Fig. 3f).

We reasoned that if the nascent polypeptide plays an active role in disengaging Reh1, shortening the length of the C-terminus of Reh1 in the exit tunnel should increase footprints of Reh1-bound ribosomes

Fig. 2 | Reh1 + 6 blocks Efl1 function. a Reh1 + 6 inhibits the GTPase activity of Efl1. Efl1 GTPase activity was monitored by the production of GDP in reactions containing the indicated combinations of 80 nM 60S subunits, 100 nM Sdo1, 60 nM Efl1 and 80 nM (1x relative to 60S) or 400 nM (5x relative to 60S) Reh1 (WT or Reh1 + 6). For reactions containing 60S, Efl1, Sdo1 and Reh1, the nonspecific GTPase activity contributed by the Reh1 preps was subtracted. Mean and standard deviation are shown. All experiments were done in triplicate. Two-tailed t-test; *P* value = 0.0443. **b** Fluorescence microscopy of Tif6-GFP expressing cells (AJY4049) containing vector or expressing *REH1* WT (pAJ4751) or *REH1 + 6* (pAJ4157). DAPI staining for nuclei and differential interference contrast (DIC) images are shown for reference. **c** Similar to panel (**a**) except strain AJY4050, expressing Nmd3-L505A-GFP, was used. **d** Reh1 + 6 does not block recycling of the upstream factors Nog1, Mrt4 and Arx1. Similar to panel (**a**) except that strains were AJY4659 (Nog1-GFP), AJY4661 (Arx1-GFP) and AJY4660 (Mrt4-GFP) and only DIC is shown for reference. **e**, The dominant negative effect of *REH1 + 6* is suppressed by *TIF6-V192F*. Ten-fold serial dilutions of wild-type yeast (BY4741) containing vectors expressing the indicated factors were plated on galactose-containing medium. Vectors used were: *REH1* (WT) pAJ4751, *REH1 + 6* (pAJ4157), vector (pRS415), *TIF6* (WT) pAJ2846, *TIF6-V192F* pAJ2249. **f** Reh1 + 6 enters polysomes when suppressed by *TIF6-V192F*. Extracts of *TIF6-V192F* mutant cells (AJY4654) expressing *REH1* WT (pAJ4751) or *REH1 + 6* (pAJ4157) were separated by sucrose density gradient sedimentation. UV trace monitoring rRNA is shown. Fractions were analyzed by western blotting for the presence of Reh1 and Rpl8. The microscopy experiments shown in panels **b**, **c** and **d** are representative cells from fields of more than 100 cells from single micrographs. The growth assay shown in panel **e** is representative of multiple isolates of each transformed strain. The experiments in panel **f** are representative of two independent experiments. Source Data are provided as a Source Data file.

deeper into coding sequence. To test this idea, we performed selective ribosome profiling on Reh1Δ6, deleted of the last 6 amino acids, a mutant that retains the ability to bind ribosomes (Supplementary Fig. 2b). Like WT Reh1, Reh1Δ6 footprints that mapped to mRNAs were predominantly 28 nucleotides in length and mapped primarily to coding sequence (Supplementary Fig. 3a,b). Intriguingly, footprints of Reh1Δ6-bound ribosomes maintained high read depth further into coding sequence compared to ribosomes bound by WT-Reh1, before the reads abruptly declined (Fig. 3g and Supplementary Fig. 3c,e). Like WT-Reh1, Reh1Δ6-bound ribosomes also showed enrichment at stop codons (Supplementary Fig. 3d). The result that shortening the C-terminus of Reh1 in the PET leads to increased persistence of ribosomes on transcripts is consistent with a model in which the growing nascent chain plays an active role in displacing Reh1.

Because Reh1 appears to bind nascent 60S subunits during their initial translation event, we asked if there was any bias for specific subsets of mRNAs translated by the Reh1-bound ribosomes (Methods). Footprints enriched for Reh1 WT and Reh1Δ6-bound ribosomes were more abundant across all mRNAs when compared to the bulk ribosome footprints (Supplementary Fig. 4a–f), suggesting that Reh1-bound ribosomes engage all mRNAs to at least some extent. This observation was expected because mRNA selection is predominantly driven by loading of the translation preinitiation complex.

Next, we wanted to understand if properties of the nascent polypeptide chain influence the release of Reh1. We found a weak but significant correlation ($\rho = 0.13$, p-value = 1.05e-20) between the net charge of the nascent polypeptide and the enrichment of footprints associated with the Reh1-bound ribosomes (Supplementary Fig. 5a,b). There was a weaker correlation with the total mass of the nascent polypeptide ($\rho = 0.06$, p-value = 2.31e-05). Taken together, these results reveal that Reh1-bound ribosomes likely engage all mRNAs yet the net charge of the nascent polypeptide of the early coding sequence slightly increases the dwell time of Reh1.

Reh1 particles are enriched for initiator tRNA

The notion that Reh1 may be evicted by the nascent polypeptide during early stages of translation together with the observation that Reh1 is enriched on mRNAs near the start codon, prompted us to ask if Reh1-bound ribosomes are enriched for initiator tRNA ($tRNA_i^{Met}$). We found that Reh1-containing ribosomes were enriched for $tRNA_i^{Met}$ relative to $tRNA_e^{Met}$ (~5-fold) and $tRNA_{UCU}^{Arg}$ when compared to the total input RNA before RNase I digestion (Supplementary Fig. 6a). Enrichment for $tRNA_i^{Met}$ relative to $tRNA_e^{Met}$ (~10-fold) was also seen when compared to RNAse I-treated extracts (Supplementary Fig. 6b). Finally, we compared the relative enrichment of tRNAs in the Reh1-bound pool to the total ribosome-bound tRNA pool. We observed a similar (~10-fold) enrichment of $tRNA_i^{Met}$ relative to $tRNA_e^{Met}$ in the Reh1-bound sample (Supplementary Fig. 6c). The enrichment of $tRNA_i^{Met}$ was also greater than the enrichment of 5S rRNA. This is consistent with a model where Reh1-bound ribosomes are enriched for $tRNA_i^{Met}$, whereas all ribosomes, free and Reh1-bound contain 5S. Both tRNAs and 5S rRNA were virtually undetectable in the untagged negative controls, showing that the RNA species were specifically associated with Reh1-bound complexes. Although we cannot know the stoichiometry of initiator tRNA in the Reh1 complexes without a standard that is fully occupied with $tRNA_i^{Met}$, our results show that Reh1-associated ribosomes are strongly enriched for initiating 80S ribosomes, consistent with our ribosome profiling analyzes.

Cryo-EM structure of the Reh1-80S complex

To gain structural insight into the nature of the Reh1-bound 80S complex, we determined the 3.1 Å cryo-EM structure of immunoprecipitated Reh1-3xFLAG bound to the translating ribosome. We used a focused 3D classification strategy to separate 80S complexes by occupancy of the A site and E site, resolving four distinct ribosomal complexes (Supplementary Fig. 7b). Two complexes were occupied by A and P site tRNAs and mRNA with eIF5A (Reh1-80S-tRNA-eIF5A, Fig. 4a) and without eIF5A (Reh1-80S-tRNA, Supplementary Fig. 8a). One complex lacked tRNAs but contained eIF5A and fragmented density consistent with the ribosome dormancy factor Stm1 (Supplementary Fig. 7b), which has previously been observed in both vacant and eIF5A-containing ribosome structures[27,28]. The fourth complex lacked tRNAs and translation factors. Our structures reveal a translating 80S complex in which the C-terminal 57 amino acids of Reh1 occupy nearly the entire length of the exit tunnel (Fig. 4a). In these structures, the C-terminus of Reh1 adopts a conformation nearly identical to that previously observed of Reh1 in the exit tunnel of pre-60S subunits[5,10]. The remaining 375 amino acids of Reh1 were not observed in any of our structures, suggesting that the C-terminus of Reh1 forms the only resolvable connection between Reh1 and the translating 80S. Reh1 may retain interaction with eL24 (Rpl24) in this state. However, the C-terminal domain of eL24 to which Reh1 is expected to bind is highly flexible and was not observed in our structures.

Nearly half of Reh1-containing 80S particles contained mRNA and tRNAs in the A and P sites. Within 42% of these 80S complexes, the essential translation factor eIF5A was also present in the E site. The unexpected observation of eIF5A reinforces the notion that Reh1-80S structures represent actively translating ribosomes captured at a relatively slow step of elongation. The critical modified amino acid of eIF5A, hypusine 51 (Hyp51), is inserted deep into the PTC E site, in proximity to the 3′ end of P site tRNA (Fig. 4b). The C-terminal residue of Reh1, glutamine 432 (Gln432), forms a stacking interaction with adenosine 2404 (A2404) of the 25S rRNA (Fig. 4c). A2404 (2062 in *E. coli* numbering) is a universally conserved residue in the ribosome, and acts as a sensor for the nascent polypeptide[29,30]. A2404 is highly flexible, adopting a closed position along the wall of the PET in the absence of nascent peptide. However, in the presence of a nascent peptide, it extends into the lumen of the PET, where it interacts with the backbone of the first amino acid of the peptidyl tRNA. Interestingly, analysis

https://doi.org/10.1038/s41467-025-55844-8

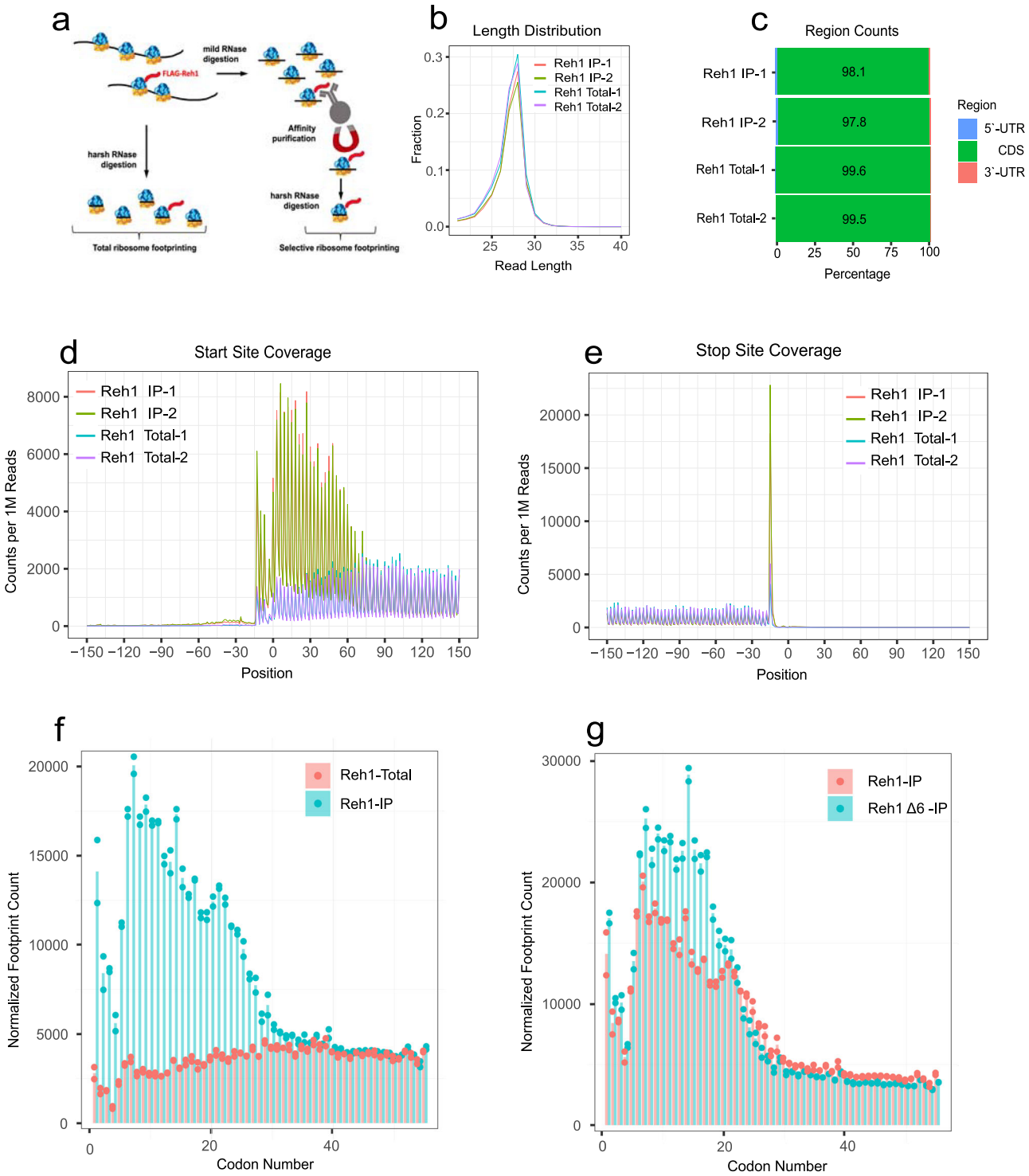

Fig. 3 | Reh1 is associated with translating ribosomes near the start codon. **a** Schematic of workflow for selective ribosome profiling. **b** The fraction of specific read lengths for the total mapped reads from selective and total ribosome footprints for WT Reh1. **c** The percentage of ribosome profiling reads across 5′-UTR, CDS, 3′-UTR regions for WT Reh1. **d** Metagene analysis of footprints mapping near the start codons for WT Reh1. Counts per million reads is plotted against nucleotide position. The position indicates the 5′ end of the footprints. **e** Metagene analysis of footprints mapping near the stop codons. **f** Distribution of reads surrounding start codons were aggregated by codon number and the mean number of reads (bar) along with individual replicates (points) were plotted for total (pink) and Reh1-bound ribosome (blue) footprints. **g** Comparison of reads from WT- and Reh1Δ6-bound ribosomes surrounding start codons. Reads were aggregated by codon number were plotted as in **f** but comparing WT Reh1 footprints (pink) with Reh1Δ6 footprints (blue). All ribosome profiling and RNA-seq experiments include two biological replicates. Source Data are provided at GEO (accession number GSE246163).

of previously published structures reveals that A2404 is in the open conformation in the presence of Reh1, even in the absence of nascent peptide, suggesting that Reh1 monitors this critical residue in the nascent subunit[5,10].

In our structures of 80S containing tRNA, the ribosomes are stalled in the pre-rotated state by cycloheximide (Supplementary Fig. 8b) which was used to prevent ribosome runoff and displacement of Reh1. In these maps, a small density that is continuous with the 3′-

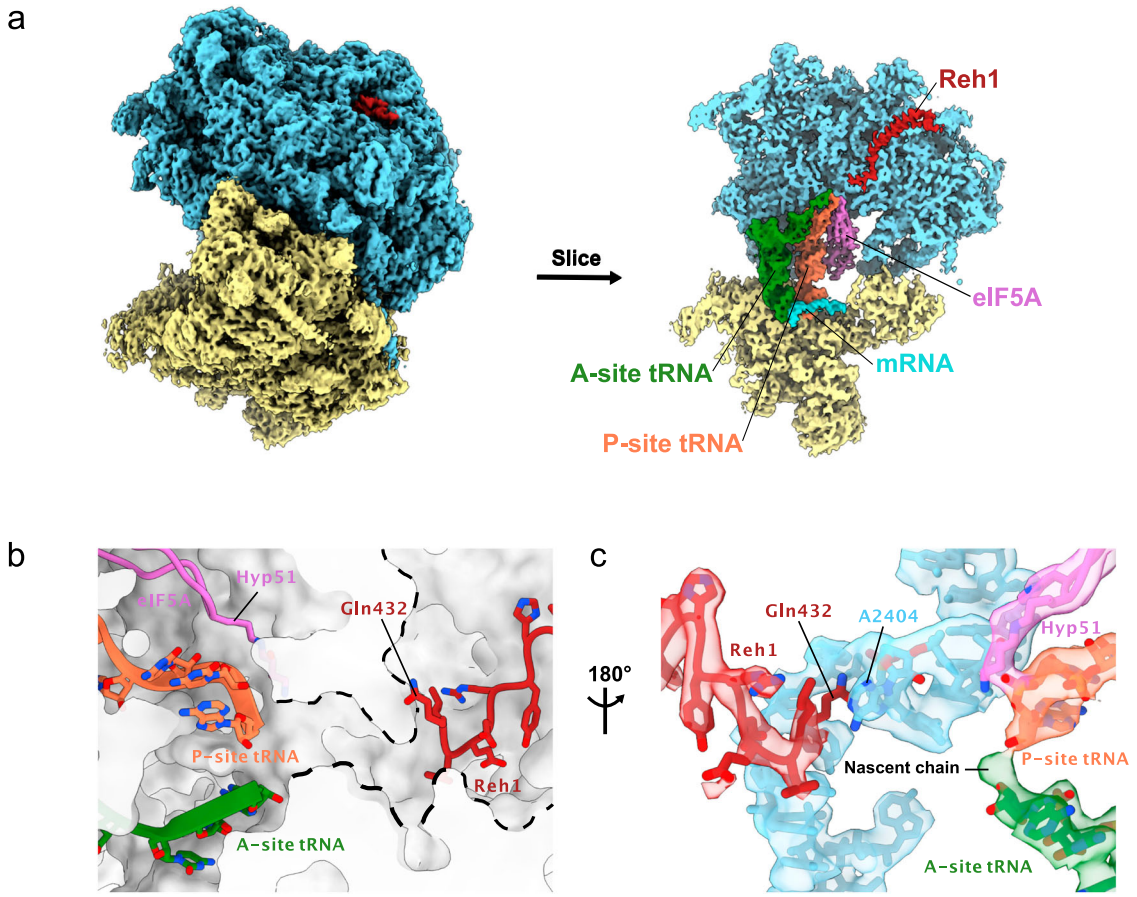

Fig. 4 | Cryo-EM structure of Reh1-bound 80S. a Cryo-EM map (left) and cross-section (right) of the eIF5A-containing Reh1-80S structure with Reh1 (red), A site tRNA (green), P site tRNA (orange), mRNA (turquoise), and eIF5A (purple). Ligands are surrounded by the large ribosomal subunit (blue) and small ribosomal subunit (yellow). **b** Cartoon representation of eIF5A, P site tRNA, and A site tRNA in the active site of Reh1-80S-tRNA-eIF5A. The PET is delineated with a dashed line. **c** Detailed view of cryo-EM map and model of Reh1-80S-tRNA-eIF5A, showing Reh1 interaction with constrictor site base A2404. Shown are Reh1 (red), A site tRNA (green), P site tRNA (orange), eIF5A (purple), and residues 2393-2407 of 25S rRNA (blue).

end of the A site tRNA, can be ascribed to the nascent chain (Fig. 4c). We could not trace a continuous density of the nascent chain to determine its length, most probably because of its dynamic and heterogeneous nature. Nevertheless, the nascent chain in this complex must be at least two amino acids long, comprising the initiating methionine and the second amino acid.

The presence of eIF5A is accompanied by closure of the L1 stalk, as seen previously[31], a shift of P site tRNA towards the A site, and slight closure of the PET around A2404 (Supplementary Movie 1). These subtle motions are potentially important for general, eIF5A-facilitated peptide bond formation. They could also be important for the release of Reh1, by decreasing the free energy of disrupting stabilizing interactions with the PET. To determine if eIF5A enhances the release of Reh1, we monitored the sedimentation of Reh1 in sucrose gradients in a conditional eIF5A mutant (*tif51a-S149P*). Shifting this mutant to the restrictive temperature of 30 °C for two hours led to a decrease in monosomes and a corresponding increase in polysomes, as reported previously (Supplementary Fig. 9a)[32]. We also observed increased Reh1 signal in polysomes at restrictive temperature. However, the distribution of Reh1 across sucrose gradients was unchanged (Supplementary Fig. 9b). We quantified the loading of Reh1 on ribosomes by sedimenting extracts through sucrose cushions and monitoring the total, free and ribosome-bound Reh1 levels relative to 60S (Supplementary Fig. 9c). Interestingly, we found that at the restrictive temperature, Reh1 was approximately 4-fold more abundant in the mutant compared to WT, accounting for the increased Reh1 signal in gradients. If eIF5A were essential for the release of Reh1, we would expect a eIF5A depletion to result in a significant shift of Reh1 from 60S to heavier fractions. However, because this shift was not observed, we conclude that eIF5A is not required for the release of Reh1.

Our structures of tRNA-containing cycloheximide-arrested ribosomes also revealed that the N-terminus of eS25 (Rps25) intercalates between the anticodon stem loop helices of the A and P site tRNAs where a series of evolutionarily-conserved lysines make backbone contacts with both tRNAs (Supplementary Fig. 8c–e). The N-terminus of eS25 is conserved throughout eukaryotes, and has been reported to interact with the IRES of Cricket Paralysis Virus during translation initiation[33]. To our knowledge, an interaction of eS25 with A and P site tRNAs has not been previously reported, but a similar interaction has been described for the C-terminus of uS19 (Rps15 in *S. cerevisiae*), which inserts between the A and P site tRNAs in cycloheximide-arrested, elongating ribosomes from human cells[34] and the filamentous fungus *N. crassa*[35]. It is tempting to speculate that the N-terminus of eS25 plays a specific role during the earliest stages of elongation, a state which we have captured with Reh1-bound ribosomes. Additional experimental work is required to test this intriguing possibility.

Discussion

Maturation of the nascent 60S subunit in yeast has been thought to culminate with the release of the subunit anti-association factor Tif6 to

license the subunit for translation[3]. Here, we have shown that the ultimate step of maturation is the release of the assembly factor Reh1 from the exit tunnel and that this step occurs after subunit joining during early cycles of translation elongation. This work adds to our current understanding of cytoplasmic maturation of the pre-60S subunit. Reh1 binds the pre-60S subunit after the release of its paralog, Rei1. Structural and crosslinking data indicate that Reh1 interacts with eL24 and Tif6 while its C-terminus inserts into the PET[5,10]. We envision that following the release of Tif6 by Sdo1 and Efl1, Reh1 remains tethered by its C-terminus in the PET and through interaction with eL24. Reh1 is evicted from the PET in early stages of translation elongation during the ribosome's first round of translation. Release from eL24 likely quickly proceeds after eviction from the exit tunnel.

Using selective ribosome profiling, we showed that Reh1-containing ribosomes are strongly enriched within the first ~75 nucleotides of coding sequences. We also observed strong enrichment for initiator $tRNA_i^{Met}$ in Reh1-bound ribosomes, and structures obtained by single-particle cryo-EM show that Reh1-bound ribosomes contain A and P site tRNAs engaged with mRNA and short nascent chains. In these structures, the only observed interaction between Reh1 and the ribosome involves the C-terminus of Reh1, which occupies the PET. This is distinct from previous structures, in which Reh1 also interacts with Tif6[5], and suggests that Reh1 in the 80S complex is primed for release. As the presence of Reh1 in the PET is incompatible with the extension of the nascent polypeptide chain, we propose that the growing nascent chain directly displaces Reh1 from the PET. We tested this model by conducting selective ribosome profiling on a short C-terminal truncation of Reh1 that retained ribosome binding (Reh1Δ6). We found that Reh1Δ6-bound ribosomes maintained high footprint counts slightly further into coding sequences. This finding is consistent with the idea that the PET can accommodate more nascent peptide before releasing Reh1, when Reh1 is shortened. It has been suggested that the entry of the nascent peptide into the PET can be facilitated by electrostatic interactions, favoring nascent peptides with a net positive charge[36]. Contrary to this, we found that nascent peptides with a net positive charge were associated with a slightly reduced rate of Reh1 release. This suggests that the presence of Reh1 in the PET may alter the electrostatic interactions of nascent peptides with the PET.

It is remarkable that in eukaryotic cells, the PET is continuously occupied from the time of its initial formation during nucleolar steps in pre-60S assembly until the first translation event of the newly assembled subunit. During early stages of 60S assembly, the C-terminus of Nog1 scaffolds elements of the PET wall to stabilize the core pre-60S complex[37]. However, when Nog1 is released from the pre-60S in the cytoplasm, the structure of the PET is complete, and it is unlikely that the subsequent insertion of Rei1 followed by Reh1 plays a similar role in stabilizing the PET. Consequently, it is an open question what function these proteins contribute by continuing to occupy the exit tunnel after its assembly. One possibility is that these proteins prevent extraneous small molecules or peptides from lodging in the ribosome before it initiates translation. Although most antibiotics target bacterial ribosomes, some can also act on eukaryotic ribosomes[38]. Small antimicrobial peptides which bind in the PET can also act on eukaryotic ribosomes[39]. Similarly, it is conceivable that endogenous, small (micro)peptides from the apparently ubiquitous translation of the genome could occupy the exit tunnel and stall translation[40]. In this scenario, Rei1 and Reh1 could keep the exit tunnel free of small molecules to ensure the unobstructed exit of the nascent polypeptide as the ribosome engages in translation.

Alternatively, Reh1 could surveil newly assembled ribosomes for function. Our results identify Reh1 as a factor that uniquely marks the 60S subunit in its initial round of translation; no other protein is known to associate exclusively with the nascent subunit to distinguish it from recycling mature subunits. If Reh1 is evicted by extension of a nascent polypeptide during a ribosome's initial round of translation, the persistence of Reh1 on the ribosome could flag it as defective and divert it to quality control or degradation pathways.

Most eukaryotic species express a single Rei1-like protein: in humans, this protein is ZNF622. Yeast and plants within the *Brassicales* are exceptions, as they express two paralogs of Rei1-like proteins that arose from independent gene duplication events. The lack of an Reh1 homolog in humans raises the question of whether ZNF622 fulfills the roles of both Rei1 and Reh1, or whether Reh1 and REIL1 in *A. thaliana* have acquired additional functions. The release of Rei1 in yeast is thought to coincide with the release of Arx1, and clearly precedes the release of Tif6. Since Rei1 physically interacts with Arx1 in the pre-60S complex, it seems reasonable to suggest that in cases where an Reh1 paralog exists, the Reh1 paralog replaces Rei1 through a higher affinity for the pre-60S lacking Arx1. The subsequent release of Tif6, which interacts with both Rei1 and Reh1, likely primes the release of Reh1 and may prevent the reassociation of Reh1 with free 60S subunits. In human cells, the levels of ZNF622 depend on the ubiquitin E3 ligase HECTD1[41]. In the absence of HECTD1, both ZNF622 and eIF6 (human Tif6) accumulate on 60S subunits, suggesting that ZNF622 stabilizes eIF6 on pre-60S subunits. This scenario is consistent with the model that ZNF622 release precedes that of eIF6, suggesting that human ZNF622 is the functional homolog of Rei1, and is unlikely to act like Reh1 in yeast.

Methods

Strains and plasmids

Strains. All strains are listed in Supplementary Table 1. AJY4049 was made by integrating PmeI-cut pAGL into a *TIF6-GFP*-expressing strain (Invitrogen). AJY3027 was constructed by sequentially crossing appropriate haploid strains originally derived from the heterozygous deletion collection (Research Genetics). The *arx1Δ::KanMX* allele was converted to *arx1Δ::NatMX* by homologous replacement using p4339[42]. To make AJY4686, the *arx1Δ::NatMX* locus was replaced with *arx1-S347P* using a CRISPR strategy to target the NatMX gene with pAJ4927. AJY4050 was made by integrating PmeI-cut pAGL into AJY4078 which in turn was made by integrating an *NMD3-L505A-GFP* HIS3MX6 cassette from pAJ3590 into the BY4741 background. AJY4408 was made by integrating PmeI-cut pAGL into BY4741. Strains AJY4659, AJY4660 and AJY4661 were made by integrating PmeI-cut pAGL into the respective GFP strains (Invitrogen). AJY4654 was made by integrating PmeI-cut pAGL into AJY4047, which in turn was made by amplifying the *TIF6-V192F-GFP::HIS3MX* locus from AJY3941[43] and integrating into BY4742. AJY4653 was made by integrating a TIF6-V192F:KlURA3 cassette into AJY4050. To make AJY4807, the KanMX locus in a spore clone from the heterozygous *rei1Δ/REI1* diploid strain (Research Genetics) was replaced with NatMX. A CRISPR strategy was then used to target the NatMX locus with pAJ4927 which was repaired using pMP004.

Plasmids. All plasmids are listed in Supplementary Table 2 and oligo nucleotides are listed in Supplementary Table 3. pAJ4155, pAJ4156 and pAJ4157 were made from pAJ4752 by inverse PCR using AJO3537, AJO3538 and AJO3539, respectively, and the common oligo AJO3551. pAJ4751 and pAJ4157 were amplified with AJO3590 and AJO1634 and the amplicons digested with EcoRI and XhoI and cloned into the EcoRI and SalI sites of pMALC2H10T to make pAJ4612 and pAJ4613, respectively. pAJ4618 *REH1* was amplified from genomic DNA using AJO3504 and AJO3505 and assembled via Golden Gate cloning with the appropriate part vectors from the Yeast Toolkit[44]. pAJ4619 was made from pAJ4618 by inverse PCR using oligos AJO3551 and AJO3539. pAJ4621 was made by cloning a fragment containing P_{GAL1}-ProtA-TEV-FLAG into

the XbaI-SacI sites of pAJ4618. To make pAJ4646, *REH1* with 500 nucleotides of upstream sequence was amplified and assembled with a *TDH1* terminator using yeast tool kit parts[44]. pAJ4942 was made by cloning the P_{REH1}-3xFLAG-*REH1*-containing EagI-XhoI fragment from pMP004[15] into pRS316. pAJ4966 and pAJ4967 were made by subcloning mutant *REH1* as SacI-XhoI segments from pAJ5501 and pAJ5503, respectively, into pAJ4646. pAJ4751 *REH1* was amplified from genomic DNA using AJO3504 and AJO3505 and assembled via Golden Gate cloning with appropriate Yeast Toolkit parts. pAJ4752: *REH1* was amplified from genomic DNA using AJO3504 and AJO3506 and assembled with the appropriate Yeast Toolkit parts. pAJ4763 was made by moving the EcoRI-BglII P_{GAL1} fragment from pAJ4751 into same sites of pAJ4753. pAJ4753 was made by cloning a gene block (IDT) containing 500 nucleotides upstream of the *REH1* start codon followed by a 3xmyc tag into the XbaI and SacI sites of pAJ4751. pAJ4764 was made by cloning a EcoRI-BglII P_{GAL1} fragment from pAJ4751 into same sites of pAJ4754 was made by cloning a gene block (IDT) containing 500 nucleotides upstream of the *REH1* start codon followed by a 3xmyc tag into the XbaI and SacI sites of pAJ4157. pAJ4927 was made by annealing oligonucleotides AJO4273 and AJO4274 and assembling into pAJ4247 using BsmB1. pAJ5501 and pAJ5503 were made by inverse PCR using pAJ4763 and oligonucleotides AJO3536 with AJO4217 and AJO4219, respectively. pAJ5513 was made by inverse PCR using pAJ4621 and oligonucleotides AJO3536 and AJO4217. *TIF6-V192F* was moved as a SacI, XhoI fragment from pRS316-*TIF6-V192F* (A Warren) into pRS415 to make pAJ2249.

Antibodies

The following antibodies were used in this study: Affinity purified anti-Nmd3[45] (Dilution 1:5,000), anti-Tif6 (K.-Y. Lo, Dilution 1:5,000), anti-Rpl8 K.-Y. Lo, (Dilution 1:40,000), c-myc 9e10 (626802, Biolegend, Dilution 1:10,000), FLAG M2 (F1804, Sigma, Dilution 1:10,000), and IRDye 680- and 800-labeled secondary antibodies (926-68071 and 926-32210, Dilution 1:15,000–1:20,000).

Protein purification

Reh1: Reh1 was expressed and purified from E coli as an MBP-fusion. BL21 (DE3) codon+ cells (Agilent) carrying pAJ4612 (WT Reh1) or pAJ4613 (Reh1 + 6) were cultured in LB medium containing 0.2% glucose, 75 ug/ml ampicillin and 25 ug/ml chloramphenicol. When cells reached OD600 = 0.4, cells were shifted to 16 °C and expression was induced with 1 mM IPTG overnight. All subsequent steps were performed at 0–4 °C. Cells were washed and resuspended in lysis buffer (40 mM Tris-HCl, pH 8.0, 500 mM NaCl, 10% glycerol, 5 mM BME, 1 mM PMSF and 1 uM each leupeptin and pepstatin). Cells were broken by sonication and the extract clarified by centrifugation at 25,000 x g for 20 min. Imidazole was added to 10 mM and protein was bound to Ni-NTA resin (Invitrogen) in bulk for 1 h. Resin was transferred to a disposable column and washed with 15 column volumes of lysis buffer supplemented with 10 mM imidazole, followed by 15 column volumes of low salt buffer (lysis buffer with NaCl reduced to 50 mM) supplemented with 20 mM imidazole. Protein was eluted with low salt buffer supplemented with 250 mM imidazole. Peak fractions were pooled, supplemented with 1 mM EDTA and 1 mM dithiothreitol (DTT) and bound to amylose resin. The resin was washed with 10 column volumes of amylose column buffer (40 mM Tris-HCl, pH 8.0, 500 mM NaCl, 10% glycerol, 1 mM EDTA, 1 mM DTT, 1 mM PMSF and 1 uM each leupeptin and pepstatin). Protein was eluted in amylose column buffer supplemented with 10 mM maltose. Peak fractions were pooled and applied to a Superose 12 column (Cytiva) equilibrated in amylose column buffer. Peak fractions were pooled and concentrated using a 30,000 mwco utrafiltration device (Amicon). Efl1, Sdo1 and 60S subunits were purified as described previously (Patchett). All protein concentrations were determined using a Qubit4 (Invitrogen).

GTPase assays

Reactions (25ul) were set up on ice with amounts of Efl1, Sdo1, Nmd3, Reh1 (WT or mutant) and 60S specified in the Fig. legend in reaction buffer (20 mM HEPES-KOH pH 7.5, 50 mM KCl, 2 mM Mg CH_3COOH, 1 mM DTT). Reactions were initiated by the addition of GTP to a final concentration of 40 uM containing a trace amount of [alpha-^{32}P]-GTP (Perkin Elmer) and incubated for 20 min at 30 °C. Reactions were quenched on ice with 6.25ul 0.5 M EDTA and 1ul of each reaction was spotted onto a PEI-cellulose thin layer chromatography plate (Sigma-Aldrich) and developed in 0.8 M CH_3COOH and 0.8 M LiCl. GTP and GDP were imaged with a storage phosphor screen on a Typhoon Phosphoimager. Data was analyzed using ImageJ software (NIH). All samples were corrected for non-enzymatic background hydrolysis. Efl1 reaction that also contained Reh1 or Reh1 + 6 were also corrected for the non-specific hydrolytic activity in the Reh1 preparations.

Sucrose density gradient sedimentation

Cultures were grown continuously overnight to OD600 of 0.3 in 250 ml of selective media or in YPD, as indicated. For transient expression, β-estradiol was added to a final concentration of 1uM and growth was continued for an additional 90-120 min. Cycloheximide (CHX) was added to a final concentration of 100 μg/ml, cultures shaken for a further 10 min at 30 °C before harvesting and storing at -80 °C. Cell pellets were washed and resuspended in 300 ul of lysis buffer (20 mM Tris·HCl, pH 7.5, 100 mM NaCl, 30 mM $MgCl_2$, 100 μg/ml cycloheximide, 200 μg/ml heparin, 5 mM β-mercaptoethanol, 1 mM PMSF and 1 μM each of leupeptin and pepstatin). Extracts were prepared by agitation with glass beads and clarified by centrifugation at 4 °C for 15 min at 18,000 x g. 10 A260 units of clarified extract were loaded onto 7-47% (w/v) sucrose gradients (containing 50 mM Tris·HCl, pH 7.5, 50 mM KCl, 12 mM $MgCl_2$, 1 mM DTT) and centrifuged for 2.5 h at 285,000 x g in a Beckman SW40 rotor. Alternatively, for gradients shown in Fig. 1 S1 and 4 S3, 50 ml cultures were grown to OD600 of 0.3-0.5, treated as indicated by temperature shift and the addition of cycloheximide and extracts were prepared immediately by agitation with glass beads in 150 ul of LHB buffer (0.1 M NaCl, 0.03 M $MgCl_2$, 0.01 M Tris·HCl pH 7.4, 100 ug/ml cycloheximide, 200 ug/ml heparin) and flash frozen. 7.5 A260 units was layered onto 7-47% (w/v) sucrose gradients prepared in TMN buffer (0.05 M Tris-Acetate pH 7.0, 0.05 M NH_4Cl, 0.012 M $MgCl_2$) and centrifuged for 2.25 h at 285,000 x g in a Beckman SW40 rotor. Gradients were fractionated using an ISCO Model 640 fractionator or a Biocomp Piston Gradient Fractionator fitted with a Triax flow cell into 600 μl fractions with continuous monitoring at 254 or 260 nm. 1.2 ml 100% ethanol was added to each fraction, mixed and stored at -20 °C overnight. Fractions were centrifuged at 4 °C for 15 min at 18,000 x g and pellets were dissolved in 1X SDS-PAGE sample buffer and heated at 99 °C for 3 mins. Proteins were separated on 6-18% gradient SDS-PAGE gels, transferred to nitrocellulose membrane and subjected to western blot analysis using the indicated antibodies as described (Antibodies).

For sucrose cushions to measure Reh1 association with ribosomes, 5 A260 units of extract in 50 ul of LHB buffer was layered over 50 ul of 17% sucrose in TMN buffer and centrifuged at 165,000 x g for 20 min at 4 °C in a TLA100 rotor (Beckman Coulter). The top 50 ul (supernatant) was removed and the pellet was resuspended in 50 ul of LHB buffer. 10% of the supernatant and pellet and an equivalent amount of total extract was analyzed by SDS-PAGE and western blotting.

Fluorescence Microscopy

Cells were grown to mid-log phase and fixed by the addition formaldehyde to 3.7% final concentration for 30 min. Cells were washed three times in cold 0.1 M potassium phosphate buffer pH 6.6 and then resuspend in 0.1 M potassium phosphate pH 6.6, 1.2 M sorbitol and

0.1% Triton X-100. DAPI was added to a final concentration of 1 ug/ml. After incubation for 1 min at room temp, cells were washed three times with cold PBS. The fluorescence signal was captured using a 500-ms exposure time on a Nikon E800 microscope fitted with a Plan Apo 100/1.4-numerical-aperture objective and a PCO sCMOS pco.edge camera controlled by NIS-Elements AR2.10 software, and photos were processed with Affinity Designer.

Ribosome Profiling Experiments and Computational Analyzes

Cultures of AJY4408 with plasmid pAJ4621 or pAJ5513 were grown to OD600 of 0.3 in 1.5 L of Leu-Glucose media by continuous overnight growth. β-estradiol was added to a final concentration of 1 uM and growth was continued for an additional 90 min. Cycloheximide (CHX) was added to a final concentration of 100 μg/ml and cultures were shaken for 10 min at 30 °C, harvested and frozen at -80 °C. Cells were washed once in IP buffer (Tris HCl 20 mM pH 7.5, 100 mM KCl, 10 mM $MgCl_2$, 100 ug/ml CHX, Pierce Protease Inhibitor Cocktail, EDTA-free (1 tablet/10 ml), 1 mM PMSF, 1 uM each leupeptin and pepstatin and 5 mM beta-mercaptoethanol (BME)) and then resuspended in a volume of IP buffer equal to that of the cell pellet. Extracts were prepared by agitation with glass beads, Igepal was added to 0.1% extracts were clarified by centrifugation at 4 °C for 15 min at 18,000 x g. 20 mg of RNA (~ 2 ml sample) was digested with 62.5 units of RNase I (Epicentre) at 4 °C for 1 h. 50 ul was removed for total Ribo-seq sample. 25 ul bed volume washed anti-FLAG magnetic beads (Sigma Milipore) was added to the remaining sample and samples were rotated for 1 h at 4 °C. Beads were washed 4 times with IP buffer supplemented with 0.1% Igepal and transferred to a clean tube during the last wash. Reh1-bound ribosomes were eluted in 100 ul of IP buffer supplemented with 0.1% Igepal and 150 ug/ml 3xFLAG peptide (Sigma Milipore) for 15 min at 4 °C. 12.5 units RNase I was added to the eluate and digestion was carried out at room temperature for 45 min. RNAse I digestion reaction was stopped by addition of QIAzol followed by RNA extraction by chloroform and ethanol precipitation.

For total RIbo-seq samples, 6.25 units RNase I (Epicentre) was added to 5ul of sample in a total volume of 50 ul in IP buffer supplemented with 0.1% Igepal. Digestion was carried out at room temperature for 45 min. Digested lysates were layered onto 50 ul 1 M sucrose cushions prepared in IP buffer and ribosomes were pelleted by centrifugation at 165,000 x g in a TLA 100 rotor (Beckman Coulter) for 30 min at 4 °C.

RNA was extracted from the ribosome pellets with the addition of 700 μl QIAzol followed by chloroform and ethanol precipitation. Isolated RNAs were size-selected using a 15% polyacrylamide TBE-UREA gel (Invitrogen) and 28-35 nt fragments were excised and extracted by crushing the gel fragment in 400 μL of RNA extraction buffer (300 mM NaOAc [pH 5.5], 5 mM $MgCl_2$). The sample was passed through a Spin X filter (Corning 8160) and the flow through was ethanol precipitated (2.5 X volume) with 1.5 μL of Glycoblue (Invitrogen AM9516). Ribosome profiling libraries were prepared as previously described[46] using the D-Plex Small RNA-Seq Kit (Diagenode). The cDNA was amplified for ten cycles. Each library was cleaned with PCR purification kit (Qiagen) and eluted with 30 μL of RNase-free water. To completely remove the primer-dimers, size-selection was done in a 3% agarose pre- cast gel (Sage Science) with the BluePippin system (Sage Science) using 180-235 nt range (tight settings, target:208 bp). The resulting size-selected libraries were analyzed with the Agilent High Sensitivity DNA Kit (Agilent). Each library was mixed in equimolar proportion for sequencing with the NovaSeq 6000 SP PE.

Ribosome profiling data was preprocessed using RiboFlow[47]. Briefly, the first 12 nucleotides were extracted and used as unique molecular identifiers. The next four nucleotides matching the sequence 'NGGG' were discarded as these were added during the template-switching reverse transcription step. Sequencing fragments containing the 3' adapter sequence AAAAAAAAAACAAAAAAAAA were retained for further analyzes. rRNA, tRNA and mRNA sequences were obtained from SGD on March 14, 2022. Sequences for the CDS (coding sequence), 5' UTR (untranslated region) and 3' UTR were merged to form the complete mRNA transcript giving us a total of 5024 transcripts. For transcripts annotated with more than one 3' UTR sequence, we randomly retained one of the sequences. The resulting reference sequences are available at https://github.com/ribosomeprofiling/yeast_reference. PCR duplicates were eliminated from the ribosome profiling data using UMI-tools[48]. Statistical analyzes and meta-gene plots were generated using RiboR using ribosome footprints of length between 26 and 29[47].

For transcript specific analyzes, ribosome footrpints whose 5' end mapped to −35 to +60 nt with respect to the start codon of all transcripts were analyzed. For each replicate of matched total ribosome profiling and Reh1 selective-ribosome profiling, the footprint counts were normalized to sequencing depth and a linear regression line was fitted. The residuals for each transcript were extracted and averaged across the replicates. This average residual corresponds to the degree of enrichment of Reh1-bound ribosomes over the total. For analyzing the effect of charge of nascent polypeptide chain on Reh1 release, a net charge was calculated for the first 20 amino acids of all transcripts (Arg, Lys +1; Glu, Asp -1). Spearman correlation was calculated between residual as described and the net charge of the first 20 amino acids. Ribograph was used to visualize read density of individual transcripts[49].

Northern blotting for tRNA enrichment

Cultures (500 ml) of yeast strain AJY4408 with plasmids pAJ4618 or pAJ4621 were grown and extracts prepared as described for Ribosome Profiling Experiments. Polysomes were collapsed to monosomes by digestion with 3 units of RNase I (Ambion) per A260 unit for 2 h at 4 °C. Immunoprecipitation was carried out by addition of ~3 mg of magnetic Dynabeads coupled with rabbit IgG[50] for 1 h at 4 °C. Beads were washed three times in IP buffer and particles eluted at 4 °C with TEV protease (prepared in house). Eluted samples were diluted into LETS buffer (0.1 M LiCl, 0.01 M EDTA, 0.01 M Tris-Cl (pH 7.4) and 0.2% SDS), extracted sequentially with phenol/CHCl3 and CHCl3, and RNA was precipitated with ethanol with addition of Glycoblue (Ambion). Input RNA samples were isolated from 7.5 A260 units before or after RNase I digestion, by phenol/CHCl3 extraction in LETS. Ribosome-bound RNA samples were prepared by sedimentation of 7.5 A260 units of RNase I-treated extract through 50 ul of 17% sucrose in IP buffer for 20' at 70,000 rpm in a Beckman TLA100 rotor at 4 °C. Pellets were resuspended in LETS and RNA was extracted with phenol/CHCl3 followed by ethanol precipitation. For northern blotting, 5 ug of total RNA or 15% of the immunoprecipitated samples was separated on a 10% TBE-Urea gel (Invitrogen), transferred to Zeta-probe (BioRad) membrane and hybridized with the indicated radiolabeled oligonucleotide probes. Probes were: $tRNA_i^{Met}$ (5'-TGGTAGCGCCGCTCGGTTTCGAATCC), $tRNA_e^{Met}$ (5'-TGCTCCAGGGGAGGTTCGAACTCTCGACC) $tRNA_{UCU}^{Arg}$ (5'-CACTCACGATGGGGGTCGAA), and 5S (5'-TCTGGTAGATATGGC CGCAACC).

Cryo-EM data collection and processing

Reh1-bound ribosomes were affinity-purified as described above for ribosome profiling, but without the second, stringent, RNAse treatment for footprinting. Samples were immediately applied to grids. Quantifoil R1.2/1.3 grids coated with an ultrathin layer of amorphous carbon (Electron Microscopy Sciences) were glow-discharged for 1 minute at 25 mA. Using a Mark IV VitroBot (Thermo Fisher Scientific), 2.5 uL of sample was applied to freshly glow-discharged grids at 4 °C and 100% humidity, immediately blotted for 2 sec at a force setting of 0, then plunged into liquid ethane and stored under liquid nitrogen

until data collection. Microscopy data were collected at the University of Texas at Austin Sauer Structural Biology Center (RRID:SCR_022951), on a Titan Krios microscope (Thermo Fisher Scientific) operating at 300 kV, equipped with a K3 Summit direct electron detector (Gatan). Movies were acquired using SerialEM v3.9[51] and recorded as 20 frames over 4 sec for a total electron dosage of ~70 e^- per $Å^2$. Movies were recorded at a nominal magnification of 29,000x, a pixel size of 0.81 Å, and over a defocus range of −1 μm to −2.5 μm. Using cryoSPARC Live v4.0[52] for on-the-fly processing, movies were motion-corrected and dose-weighted, and CTF estimates performed. Particles of diameter between 300 Å and 400 Å were selected using a circular blob picker. On-the-fly 2D classification was used to separate particles in clean 80S and pre-60S classes, which were then exported to cryoSPARC v3.2, where multiple subsequent rounds of 2D classification resulted in a total of 217,663 particles corresponding to 80S and pre-60S projections. These particles were used for ab initio reconstruction and 3D heterogeneous refinement into separate 80S and pre-60S classes of 115,111 and 92,218 particles, respectively.

The pre-60S class showed complete or partial occupancy for cytoplasmic ribosome assembly factors, including Tif6, Nmd3, Lsg1 and Reh1, but further analysis was precluded by severe orientation bias. The well-resolved 80S class was further subjected to a two-part 3D classification scheme in cryoSPARC v3.2, with a soft mask surrounding the A site followed by a soft mask surrounding the E site. This scheme led to four 80S classes containing A and P site tRNAs, and/or E site eIF5A (Supplementary Fig. 7b). The local resolution of the two maps containing tRNA was determined using Local Resolution Estimation in CryoSPARC v3.2, with default parameters.

Modeling, refinement and graphics

PDB 7NRC[53] was first rigid-body docked into the two maps with resolved tRNAs, with and without eIF5A. The model for Reh1 was derived from PDB 6QTZ[5]. A predicted model for yeast Rps25-A (AF-Q3E792-F1) was downloaded from the AlphaFold Protein Structure Database[54,55], and its N-terminus was fit manually into the EM map using COOT v1.1.10[56]. The mRNA chain was built manually in COOT. Models were relaxed using flexible fitting implemented in ISOLDE v1.4[57], then subjected to real-space refinement implemented in PHENIX v.1.19[58]. Refinement statistics are provided in Supplementary Table 4. Molecular graphics were prepared using UCSF ChimeraX v1.720[59].

Reporting summary

Further information on research design is available in the Nature Portfolio Reporting Summary linked to this article.

Data availability

Sequencing files for selective ribosome profiling experiments are available at GEO (accession number GSE246163). The structures of Reh1-80S-tRNA-eIF5A and Reh1-80S-tRNA have been deposited in the Electron Microscopy Data Bank as EMDB-42545[https://www.ebi.ac.uk/emdb/EMD-42525] and EMDB-42540[https://www.ebi.ac.uk/emdb/EMD-42540], respectively. The corresponding molecular models of Reh1-80S-tRNA-eIF5A and Reh1-80S-tRNA have been deposited in the Protein Data Bank as PDB-8UT0[https://doi.org/10.2210/pdb8ut0/pdb] and PDB-8UTI[https://doi.org/10.2210/pdb8uTi/pdb], respectively. Source data are provided with this paper.

References

1. Klinge, S. & Woolford, J. L. Ribosome assembly coming into focus. *Nat. Rev. Mol. Cell Biol.* **20**, 116–131 (2019).
2. Baßler, J. & Hurt, E. Eukaryotic Ribosome Assembly. *Annual Review of Biochemistry* https://doi.org/10.1146/annurev-biochem-013118 (2019).
3. Dörner, K., Ruggeri, C., Zemp, I. & Kutay, U. Ribosome biogenesis factors—from names to functions. *EMBO J.* **42**, e112699 (2023).
4. Peña, C., Hurt, E. & Panse, V. G. Eukaryotic ribosome assembly, transport and quality control. *Nature Structural and Molecular Biology* **24**, 689–699 (2017).
5. Kargas, V. et al. Mechanism of completion of peptidyltransferase centre assembly in eukaryotes. *Elife* **8**, 1–26 (2019).
6. Zhou, Y., Musalgaonkar, S., Johnson, A. W. & Taylor, D. W. Tightly-orchestrated rearrangements govern catalytic center assembly of the ribosome. *Nat. Commun.* **10**, 958 (2019).
7. Espinar-Marchena, F. J., Babiano, R. & de la Cruz, J. Placeholder factors in ribosome biogenesis: Please, pave my way. *Microbial Cell* **4**, 144–168 (2017).
8. Wu, S. et al. Diverse roles of assembly factors revealed by structures of late nuclear pre-60S ribosomes. *Nature* **534**, 133–137 (2016).
9. Lo, K.-Y. et al. Defining the pathway of cytoplasmic maturation of the 60S ribosomal subunit. *Mol Cell* **39** (2010).
10. Ma, C. et al. Structural snapshot of cytoplasmic pre-60S ribosomal particles bound by Nmd3, Lsg1, Tif6 and Reh1. *Nat. Struct. Mol. Biol.* **24**, 214–220 (2017).
11. Klingauf-Nerurkar, P. et al. The gtpase nog1 co-ordinates the assembly, maturation and quality control of distant ribosomal functional centers. *Elife* **9**, e52474 (2020).
12. Greber, B. J., Boehringer, D., Montellese, C. & Ban, N. Cryo-EM structures of Arx1 and maturation factors Rei1 and Jjj1 bound to the 60S ribosomal subunit. *Nat. Struct. Mol. Biol.* **19**, 1228–1233 (2012).
13. Demoinet, E., Jacquier, A., Lutfalla, G. & Fromont-Racine, M. The Hsp40 chaperone Jjj1 is required for the nucleo-cytoplasmic recycling of preribosomal factors in Saccharomyces cerevisiae. *RNA* **13**, 1570–1581 (2007).
14. Meyer, A. E., Hoover, L. A. & Craig, E. A. The Cytosolic J-protein, Jjj1, and Rei1 Function in the Removal of the Pre-60 S Subunit Factor Arx1. *J. Biol. Chem.* **285**, 961–968 (2010).
15. Parnell, K. M. & Bass, B. L. Functional Redundancy of Yeast Proteins Reh1 and Rei1 in Cytoplasmic 60S Subunit Maturation. *Mol. Cell Biol.* **29**, 4014–4023 (2009).
16. Finch, A. J. et al. Uncoupling of GTP hydrolysis from eIF6 release on the ribosome causes Shwachman-Diamond syndrome. *Genes Dev.* **25**, 917–929 (2011).
17. Bussiere, C., Hashem, Y., Arora, S., Frank, J. & Johnson, A. W. Integrity of the P-site is probed during maturation of the 60S ribosomal subunit. *J. Cell Biol.* **197**, 747–759 (2012).
18. Sailer, C. et al. A comprehensive landscape of 60S ribosome biogenesis factors. *Cell Rep* **38** (2022).
19. Olga, B. G. et al. Plant temperature acclimation and growth rely on cytosolic ribosome biogenesis factor homologs. *Plant Physiol.* **176**, 2251–2276 (2018).
20. Menne, T. F. et al. The Shwachman-Bodian-Diamond syndrome protein mediates translational activation of ribosomes in yeast. *Nat. Genet* **39**, 486–495 (2007).
21. Hung, N.-J., Lo, K.-Y., Patel, S. S., Helmke, K. & Johnson, A. W. Arx1 is a nuclear export receptor for the 60S ribosomal subunit in yeast. *Mol. Biol. Cell* **19**, 735–744 (2008).
22. Lebreton, A. et al. A functional network involved in the recycling of nucleocytoplasmic pre-60S factors. *J. Cell Biol.* **173**, 349–360 (2006).
23. Hung, N.-J. & Johnson, A. W. Nuclear recycling of the pre-60S ribosomal subunit-associated factor Arx1 depends on Rei1 in Saccharomyces cerevisiae. *Mol Cell Biol* **26** (2006).
24. Greber, B. J. et al. Insertion of the Biogenesis Factor Rei1 Probes the Ribosomal Tunnel during 60S Maturation. *Cell* **164**, 91–102 (2016).
25. Duc, K. D., Batra, S. S., Bhattacharya, N., Cate, J. H. D. & Song, Y. S. Differences in the path to exit the ribosome across the three domains of life. *Nucleic Acids Res* **47**, 4198–4210 (2019).
26. Wilson, D. N. & Beckmann, R. The ribosomal tunnel as a functional environment for nascent polypeptide folding and translational stalling. *Current Opinion in Structural Biology* vol. 21, 274–282 (2011).

27. Ben-Shem, A. et al. The structure of the eukaryotic ribosome at 3.0 Å resolution. *Science (1979)* **334**, 1524–1529 (2011).
28. Melnikov, S. et al. Crystal Structure of Hypusine-Containing Translation Factor eIF5A Bound to a Rotated Eukaryotic Ribosome Correspondence to https://doi.org/10.1016/j.jmb.2016.05.011 (2016).
29. Vazquez-Laslop, N., Thum, C. & Mankin, A. S. Molecular Mechanism of Drug-Dependent Ribosome Stalling. *Mol Cell* **30** (2008).
30. Syroegin, E. A., Aleksandrova, E. V. & Polikanov, Y. S. Insights into the ribosome function from the structures of non-arrested ribosome–nascent chain complexes. *Nat. Chem.* **15**, 143–153 (2023).
31. Schmidt, C. et al. Structure of the hypusinylated eukaryotic translation factor eIF-5A bound to the ribosome. *Nucleic Acids Res* **44**, 1944–1951 (2016).
32. Saini, P., Eyler, D. E., Green, R. & Dever, T. E. Hypusine-containing protein eIF5A promotes translation elongation. *Nature* **459**, 118–121 (2009).
33. Walters, B., Axhemi, A., Jankowsky, E. & Thompson, S. R. Binding of a viral IRES to the 40S subunit occurs in two successive steps mediated by eS25. *Nucleic Acids Res* **48**, 8063–8073 (2020).
34. Bhaskar, V. et al. Dynamics of uS19 C-Terminal Tail during the Translation Elongation Cycle in Human Ribosomes In Brief. https://doi.org/10.1016/j.celrep.2020.03.037.
35. Shen, L. et al. Structure of the translating *Neurospora* ribosome arrested by cycloheximide. *Proceedings of the National Academy of Sciences* **118** (2021).
36. Dao Duc, K. & Song, Y. S. The impact of ribosomal interference, codon usage, and exit tunnel interactions on translation elongation rate variation. *PLoS Genet* **14** (2018).
37. Wilson, D. M. et al. Structural insights into assembly of the ribosomal nascent polypeptide exit tunnel. https://doi.org/10.1038/s41467-020-18878-8.
38. Dmitriev, S. E., Vladimirov, D. O. & Lashkevich, K. A. A Quick Guide to Small-Molecule Inhibitors of Eukaryotic Protein Synthesis. *Biochemistry (Moscow)* **85**, 1389–1421 (2020).
39. Seefeldt, A. C. et al. Structure of the mammalian antimicrobial peptide Bac7(1-16) bound within the exit tunnel of a bacterial ribosome. *Nucleic Acids Res* **44**, 2429–2438 (2016).
40. Wacholder, A. et al. A vast evolutionarily transient translatome contributes to phenotype and fitness. *Cell Syst.* **14**, 363–381.e8 (2023).
41. Lv, K. et al. HectD1 controls hematopoietic stem cell regeneration by coordinating ribosome assembly and protein synthesis. *Cell Stem Cell* **28**, 1275–1290.e9 (2021).
42. Goldstein, A. L. & McCusker, J. H. Three new dominant drug resistance cassettes for gene disruption inSaccharomyces cerevisiae. *Yeast* **15**, 1541–1553 (1999).
43. Patchett, S., Musalgaonkar, S., Malyutin, A. G. & Johnson, A. W. The T-cell leukemia related rpl10-R98S mutant traps the 60S export adapter Nmd3 in the ribosomal P site in yeast. *PLoS Genet* **13**, e1006894 (2017).
44. Lee, M. E., DeLoache, W. C., Cervantes, B. & Dueber, J. E. A Highly Characterized Yeast Toolkit for Modular, Multipart Assembly. *ACS Synth. Biol.* **4**, 975–986 (2015).
45. Ho, J. H.-N., Kallstrom, G. & Johnson, A. W. Nascent 60S ribosomal subunits enter the free pool bound by Nmd3p. *RNA* **6**, S1355838200001291 (2000).
46. Rao, S. et al. Genes with 5′ terminal oligopyrimidine tracts preferentially escape global suppression of translation by the SARS-CoV-2 Nsp1 protein. *RNA* **27**, 1025–1045 (2021).
47. Ozadam, H., Geng, M. & Cenik, C. Gene expression RiboFlow, RiboR and RiboPy: an ecosystem for analyzing ribosome profiling data at read length resolution. https://doi.org/10.1093/bioinformatics/btaa028.
48. Smith, T., Heger, A. & Sudbery, I. UMI-tools: modeling sequencing errors in Unique Molecular Identifiers to improve quantification accuracy. https://doi.org/10.1101/gr.209601.116 (2017).
49. Chacko, J., Ozadam, H. & Cenik, C. RiboGraph: an interactive visualization system for ribosome profiling data at read length resolution. https://doi.org/10.1093/bioinformatics/btae369 (2024).
50. Oeffinger, M. et al. Comprehensive analysis of diverse ribonucleoprotein complexes. *Nat. Methods* **4**, 951–956 (2007).
51. Mastronarde, D. N. Automated electron microscope tomography using robust prediction of specimen movements. *J. Struct. Biol.* **152**, 36–51 (2005).
52. Punjani, A., Rubinstein, J. L., Fleet, D. J. & Brubaker, M. A. CryoSPARC: Algorithms for rapid unsupervised cryo-EM structure determination. *Nat Methods* **14**, 290–296 (2017).
53. Pochopien, A. A. et al. Structure of Gcn1 bound to stalled and colliding 80S ribosomes. *Proceedings of the National Academy of Sciences* **118** (2021).
54. Varadi, M. et al. NAR Breakthrough Article AlphaFold Protein Structure Database: massively expanding the structural coverage of protein-sequence space with high-accuracy models. *Nucleic Acids Res* **50** (2021).
55. Jumper, J. et al. Highly accurate protein structure prediction with AlphaFold. *Nature* **596**, 583–589 (2021).
56. Emsley, P., Lohkamp, B., Scott, W. G. & Cowtan, K. Biological Crystallography Features and development of Coot. https://doi.org/10.1107/S0907444910007493.
57. Croll, T. I. ISOLDE: a physically-realistic environment for model building into low-resolution electron-density maps. **74**, 519–530 (2018).
58. Liebschner, D. et al. Macromolecular structure determination using X-rays, neutrons and electrons: recent developments in Phenix. *Acta Cryst.* **75**, 861–877 (2019).
59. Pettersen, E. F. et al. UCSF ChimeraX: Structure visualization for researchers, educators, and developers. *Protein Sci.* **30**, 70–82 (2021).
60. Weis, F. et al. Mechanism of eIF6 release from the nascent 60S ribosomal subunit. *Nat. Struct. Mol. Biol.* **22**, 914–919 (2015).

Acknowledgements

This work was supported by NIH grants GM127127 (to A.W.J.) GM138348 (to D.W.T). and GM150667 (to CC), and Welch Foundation Research Grants F-1938 (to D.W.T) and F-2027-20230405 (to C.C.). C.C. is a CPRIT Scholar in Cancer Research supported by the Cancer Prevention and Research Institute of Texas grant RR180042. We thank D. Gottschling for pAGL, J. Tesmer for pMALC2H10T, B. Bass for pMP004, J. Dueber for yeast toolkit vectors and K.-Y. Lo for rabbit anti-Rpl8 and anti-Tif6 antibody.

Author contributions

S.M. conceived the experiments, performed genetic and biochemical analyzes, fluorescence microscopy and prepared samples for cryo-EM and RNA analysis. J.N.Y performed cryo-electron microscopy, structure determination and modeling. R.C. performed genetic and biochemical analyzes and prepared samples for RNA analysis. S.R. performed and analyzed ribosome profiling experiments. H.O. set up the analysis pipeline for ribosome profiling experiments. D.W.T. analyzed the data, supervised the structural studies and obtained funding for the work. C.C. analyzed the data, obtained funding for the work and supervised ribosome profiling experiments. A.W.J. conceived the experiments, performed genetic and biochemical analyzes, analyzed the data and obtained funding for the work. All authors contributed to writing the manuscript.

Competing interests
The authors declare no competing interests.

Additional information
Supplementary information The online version contains supplementary material available at https://doi.org/10.1038/s41467-025-55844-8.

Correspondence and requests for materials should be addressed to Can Cenik or Arlen W. Johnson.

Peer review information *Nature Communications* thanks Katrin Karbstein, and the other, anonymous, reviewer(s) for their contribution to the peer review of this work. A peer review file is available.